nature nanotechnology

LETTERS

PUBLISHED ONLINE: 28 MARCH 2016 | DOI: 10.1038/NNANO.2016.30

Single-nanowire photoelectrochemistry

Yude Su[1†], Chong Liu[1,2†], Sarah Brittman[1,2], Jinyao Tang[1,2], Anthony Fu[1,2], Nikolay Kornienko[1,2], Qiao Kong[1] and Peidong Yang[1,2,3,4*]

Photoelectrochemistry[1–3] is one of several promising approaches[4,5] for the realization of efficient solar-to-fuel conversion. Recent work has shown that photoelectrodes made of semiconductor nano-/microwire arrays can have better photoelectrochemical performance[6–8] than their planar counterparts because of their unique properties, such as high surface area[9–11]. Although considerable research effort has focused on studying wire arrays, the inhomogeneity in the geometry, doping, defects and catalyst loading present in such arrays can obscure the link between these properties and the photoelectrochemical performance of the wires, and correlating performance with the specific properties of individual wires is difficult because of ensemble averaging. Here, we show that a single-nanowire-based photoelectrode platform can be used to reliably probe the current–voltage (*I–V*) characteristics of individual nanowires. We find that the photovoltage output of ensemble array samples can be limited by poorly performing individual wires, which highlights the importance of improving nanowire homogeneity within an array. Furthermore, the platform allows the flux of photogenerated electrons to be quantified as a function of the lengths and diameters of individual nanowires, and we find that the flux over the entire nanowire surface (7–30 electrons nm^{-2} s^{-1}) is significantly reduced as compared with that of a planar analogue (~1,200 electrons nm^{-2} s^{-1}). Such characterization of the photogenerated carrier flux at the semiconductor/electrolyte interface is essential for designing nanowire photoelectrodes that match the activity of their loaded electrocatalysts.

Devices composed of single nanowires have previously been used in electronics[12], bioprobing[13], photovoltaics[14,15], thermoelectrics[16] and electrochemistry[17]. In this Letter, we develop a single-semiconductor-nanowire device (Fig. 1a) for photoelectrochemistry that is capable of detecting solar-powered proton reduction with picoampere sensitivity. As a model system, silicon[18–21] and platinum[22] are selected as the light-absorbing semiconductor and proton-reduction electrocatalyst, respectively. Silicon nanowires were grown epitaxially on a prepatterned, degenerately doped silicon ⟨111⟩ device layer on a silicon-on-insulator (SOI) substrate, as shown in the scanning electron microscope (SEM) image in Fig. 1b. With an oxide layer underneath, the patterned silicon electrodes are electrically isolated from each other, enabling the characterization of each nanowire individually. Moreover, the vapour–liquid–solid (VLS) growth allowed control over the dimensions of the nanowire[23], which facilitated studying the effects of nanowire geometry. The as-grown single silicon nanowires were 8–20 μm long and 500–800 nm in diameter. The post-growth fabrication process yielded nanowires with two types of doping profile (Fig. 2a). In the first case, the as-grown silicon nanowires were doped into p-type only. In the second case, after p-type doping, an n^+ shell was added to yield an n^+p buried junction in each single nanowire. For both types of device, platinum nanoparticles were deposited electrolessly[22] onto the exposed nanowire (Supplementary Figs 2 and 3) after a protective polymer coating was added to the base of the wire. A specialized photoelectrochemical (PEC) measurement set-up was also developed (Fig. 2b) for high-sensitivity electrochemical characterization coupled with simulated sunlight. This unique measurement platform can be further applied to other light-driven redox reactions that require high sensitivity.

Our approach provides us with a nanowire photoelectrode platform that is individually addressable and allows single-nanowire photoelectrochemistry to be observed. The photocurrents of devices were characterized with picoampere sensitivity (Fig. 3a). In the dark, devices show negligible current ($|I| < 1$ pA). The slightly increased current at potentials to the negative of 0 V versus the reversible hydrogen electrode (RHE) implies a proton-reduction reaction catalysed by the loaded platinum nanoparticles (Supplementary Fig. 5). Under one sun illumination (100 mW cm^{-2}, AM 1.5G), a significant photoresponse was observed, with the photocurrent reaching a plateau under negative bias, indicative of a light-activated process limited by the number of incident photons. Such PEC behaviour is consistent with that of reported ensemble systems[18,19], confirming the observation of PEC phenomena at the single-nanowire level. Additionally, the performance of the device was consistent for multiple scan cycles (Fig. 3b).

The photovoltage distribution statistics of the single-nanowire devices was analysed next. For silicon photocathodes, a previous study on ensemble systems proposed that the n^+p buried junction increases the degree of band bending at the interface and consequently leads to a 250–350 mV improvement in photovoltage[18]. This concept was also implemented in our single-nanowire photoelectrodes (Supplementary Scheme 1). The onset potentials and standard deviations of p-Si and n^+p-Si devices are 280 ± 110 mV and 530 ± 120 mV versus RHE, respectively (Fig. 3c). The ~250 mV difference between the average onset potentials demonstrates that the doping profile and photovoltage of the single-nanowire photoelectrode can be reproducibly modulated. In addition, for devices that underwent the same growth and doping process, the broad photovoltage distribution implies individual variance among single nanowires. To investigate the impact of such variance, we carried out PEC measurements on ensemble nanowire arrays (Supplementary Fig. 6) in which many individual nanowires were connected in parallel. It was found that the V_{oc} of the array device is comparable with that of the single nanowire with the lowest photovoltage output (Supplementary Fig. 7), and this observation applied to both p-Si and n^+p-Si devices (Supplementary Fig. 8 and Supplementary Table 1). These results suggest that the photovoltage of the ensemble array photoelectrode is largely affected by the worst-performing individual nanowire, and this conclusion is further supported by our calculation based on an equivalent circuit model (Supplementary Fig. 9). Because the single nanowires

[1]Department of Chemistry, University of California, Berkeley, California 94720, USA. [2]Materials Sciences Division, Lawrence Berkeley National Laboratory, Berkeley, California 94720, USA. [3]Department of Materials Science and Engineering, University of California, Berkeley, California 94720, USA. [4]Kavli Energy Nanosciences Institute, Berkeley, California 94720, USA. †These authors contributed equally to this work. *e-mail: p_yang@berkeley.edu

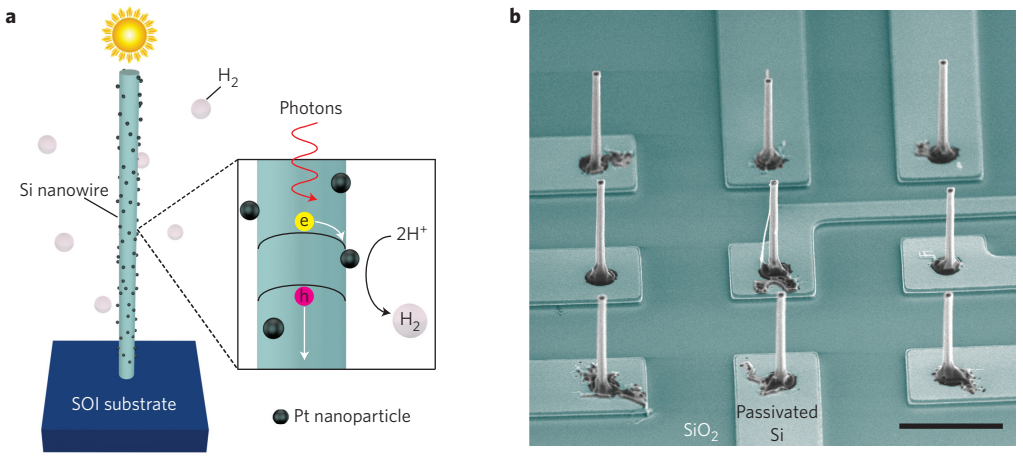

Figure 1 | Single-nanowire photoelectrode for PEC measurements. a, Schematic of the single silicon nanowire for the PEC process. Under illumination, photoexcited electron–hole pairs are produced and subsequently separated at the nanowire/electrolyte interface because of band bending. The electrons then move to the platinum catalytic sites and carry out proton reduction. **b**, SEM image of individually addressable single nanowires. The silicon layer of the SOI substrate is patterned into nine electrically isolated, oxide-passivated electrodes, with an oxide layer underneath. The single silicon nanowires are vertically grown on these isolated silicon electrodes by the VLS mechanism[23]. Scale bar, 10 μm.

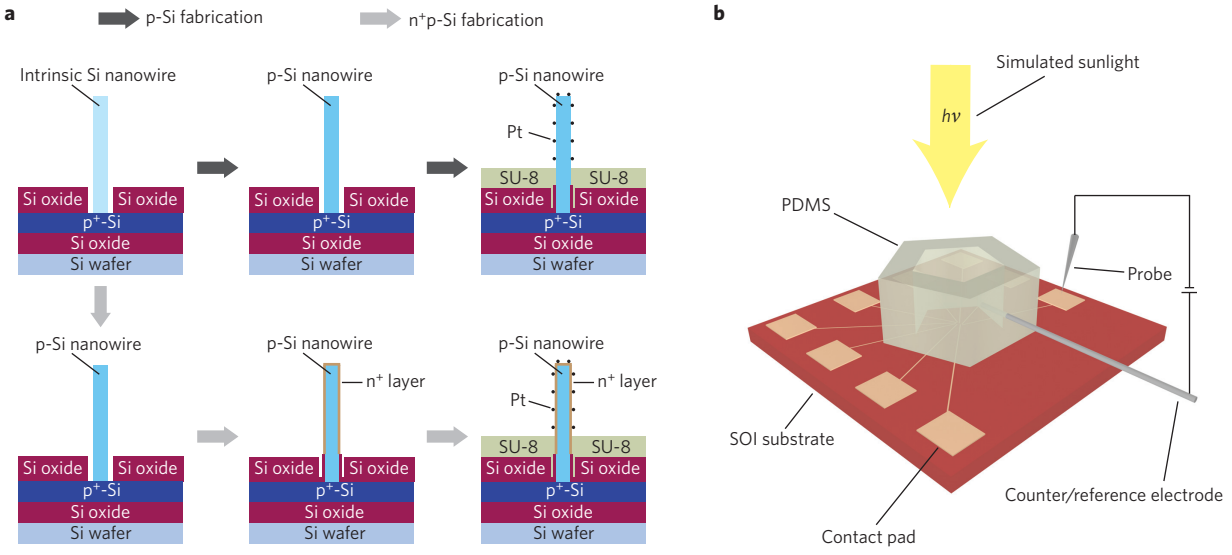

Figure 2 | Schematic illustrations of the fabrication and measurement processes. a, Outline of the post-growth fabrication process (see Methods and Supplementary Fig. 1 for details). Devices with two kinds of doping profile (p-Si and n^+p-Si) were fabricated for comparison. **b**, The PEC measurement scheme. A two-electrode configuration is used to characterize the *I*–*V* properties of single nanowires. The silicon nanowire serves as the working electrode, and a platinum wire functions as the counter/reference electrode (with its electrochemical potential calibrated) (Supplementary Fig. 4). The reactor volume in which the PEC processes occur is defined by a polydimethylsiloxane (PDMS) chamber. A probe makes electrical contact with each nanowire through the outside pads, and the chamber is illuminated from above.

and the nanowire arrays studied in this work have similar physical dimensions and go through the same doping process, such observed individual variance should be related to the heterogeneity of the material quality introduced during either the VLS growth[24,25] or the fabrication process, or both. As a result, our report emphasizes the importance of controlling the material quality, not only for the averaged value but also the sample homogeneity, to produce efficient nanowire-based solar-to-fuel devices.

Owing to the high-sensitivity photocurrent measurement and the well-defined geometry of a single nanowire, the photogenerated electron flux through the nanowire's entire surface ($\mathrm{Flux_{wire}}$) was quantified. Because of the large surface area of the nanowire, $\mathrm{Flux_{wire}}$ was much reduced compared with a planar analogue. To quantitatively evaluate how the large surface area functions to dilute the electron flux, we investigated the roughness factor of a single nanowire (γ_{rough}), given by

$$\gamma_{\mathrm{rough}} = \frac{\text{actual surface area of a single nanowire}}{\text{cross-sectional area of a single nanowire}} = \frac{4L}{D} + 1 \quad (1)$$

where the nanowire is considered to be a cylinder with length L and diameter D.

Subsequently, $\mathrm{Flux_{wire}}$ can be correlated with $\mathrm{Flux_{geo}}$, which is the photogenerated electron flux normalized to the geometric cross-sectional area:

$$\mathrm{Flux_{wire}} = \frac{\mathrm{Flux_{geo}}}{\gamma_{\mathrm{rough}}} \quad (2)$$

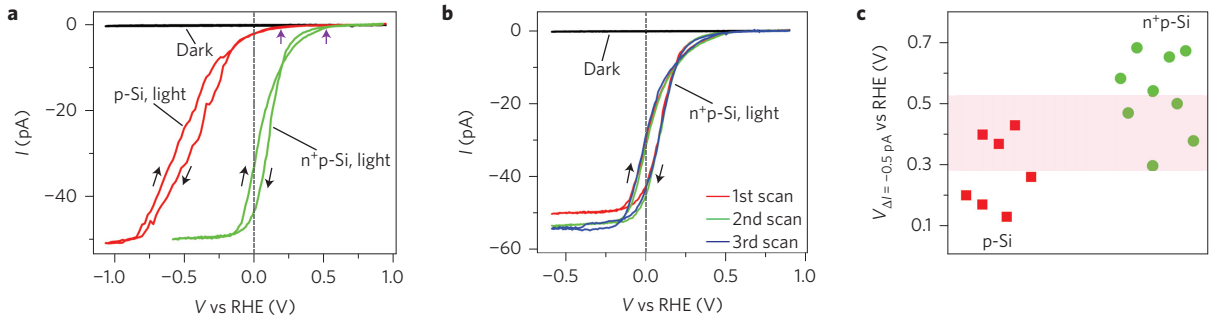

Figure 3 | PEC performance of the single-silicon-nanowire devices. a, *I*–*V* characteristics of single-nanowire devices. The measurement was carried out in 0.1 M K_2SO_4 solution adjusted to a pH of ~2 with H_2SO_4. Under simulated sunlight (100 mW cm^{-2}, AM 1.5G), both the p-Si device (L = 8 μm, D = 620 nm) and n^+p-Si device (L = 12.5 μm, D = 530 nm) have significant photoresponses. Purple arrows indicate the onsets of photocurrent as defined in **c**. **b**, Repeated scans of the n^+p-Si device displayed in **a**. **c**, Statistical distribution of onset potentials for seven p-Si and nine n^+p-Si devices. To evaluate the photovoltage response of the single-nanowire devices, the onset potential is defined as the potential versus RHE, where ΔI is −0.5 pA. ΔI is the difference between the photocurrent and the dark current. The pink band shows the difference in the average onset potential between p-Si and n^+p-Si devices.

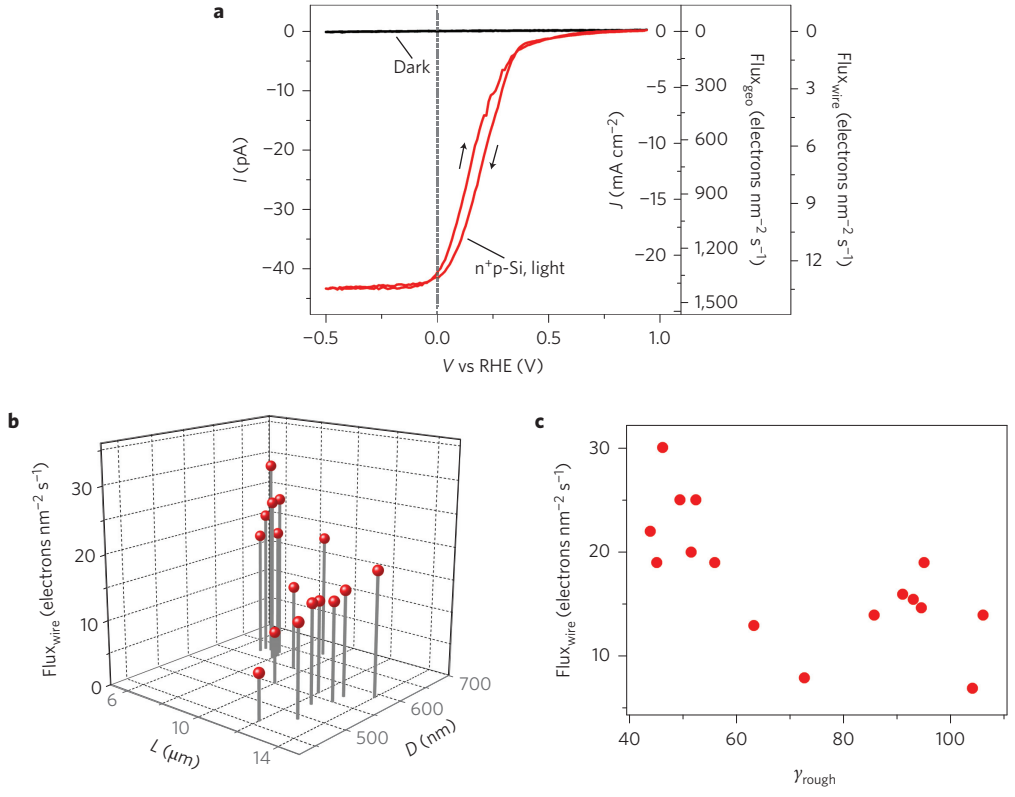

Figure 4 | Analysis of the flux of photogenerated electrons. a, PEC behaviour of a representative n^+p-Si device (L = 13 μm, D = 490 nm). The four *y* axes represent (from left to right) the recorded photocurrent (I), the current density based on the geometric cross-sectional area (J), the electron flux normalized to the geometric cross-sectional area ($Flux_{geo}$) and the electron flux through the entire surface of the nanowire ($Flux_{wire}$). **b**, Statistical distribution of saturated $Flux_{wire}$ as a function of L and D of individual nanowires. Each data point represents a repeatable measurement of one single-nanowire device. **c**, Dependence of saturated $Flux_{wire}$ on the roughness factor of individual nanowires (γ_{rough}).

Therefore $Flux_{wire}$ can be expressed as a function of L and D, which allows for a quantitative calculation of $Flux_{wire}$ for each single-nanowire device. For a representative device (Fig. 4a), I reaches a plateau of −43 pA when cathodic bias is applied. Correspondingly, J and $Flux_{geo}$ are −22 mA cm^{-2} and 1,350 electrons nm^{-2} s^{-1}, respectively (−1 mA cm^{-2} = 62 electrons nm^{-2} s^{-1}). When normalizing to the actual surface area of the nanowire, the corresponding $Flux_{wire}$ is dramatically reduced to 13 electrons nm^{-2} s^{-1}, because of the large γ_{rough}. Compared with the photogenerated electron flux of a planar n^+p-Si electrode (1,240 electrons nm^{-2} s^{-1} at 0 V versus RHE, Supplementary Fig. 10), $Flux_{wire}$ is diluted by a factor of about 100. The trend of such a reduced electron flux can be observed when values of saturated $Flux_{wire}$ for individual nanowires are plotted against their L and D (Fig. 4b). Here, we take advantage of the fact that the dimensions of each single nanowire are not only highly tunable, but can also be reliably measured, in contrast to the inhomogeneity that typically occurs in ensemble devices. Ranging from 30 to 7 electrons nm^{-2} s^{-1}, $Flux_{wire}$ follows a generally decreasing trend as L becomes longer or D becomes smaller (Supplementary Fig. 11). Such dependence can be clearly seen when $Flux_{wire}$ is correlated with γ_{rough}, which incorporates the impact of both L and D (Fig. 4c). $Flux_{wire}$ tends to decrease as

γ_{rough} increases. The effective reduction of electron flux on the nanowire surface can be estimated by considering the light absorption within a cylindrical silicon absorber and is found to scale with the γ_{rough} of the individual nanowires (Supplementary Fig. 13).

The characterization of $Flux_{wire}$ provides quantitative insight into the benefits of nanowire geometry in photoelectrochemistry. In principle, the loaded electrocatalyst should have a sufficiently high turnover frequency (TOF) to handle the photogenerated electron flux[11]. As a result, the much reduced $Flux_{wire}$ (7–30 electrons nm^{-2} s^{-1} under one sun illumination measured in this study, compared with typical ~1,200 electrons nm^{-2} s^{-1} for a planar photoelectrode) can significantly alleviate the requirement on the TOFs of loaded electrocatalysts and consequently reduce the necessary overpotential when compared with a planar counterpart (see Supplementary Table 2 for specific values). This is especially critical for more complicated and sluggish electrochemical reactions such as CO_2 reduction[26,27], where the electrocatalyst typically needs a large overpotential to reach an appreciable TOF[28–30]. In addition, the systematic trend of $Flux_{wire}$ introduces the possibility to design specific nanowire geometries to match the activities of different loaded electrocatalysts in different PEC reactions. This single-nanowire photoelectrode represents a model system that can be used to study and design nanowire photoelectrodes for next-generation solar-to-fuel conversion devices.

Methods

Methods and any associated references are available in the online version of the paper.

Received 3 April 2015; accepted 11 February 2016; published online 28 March 2016

References

1. Bard, A. J. Photoelectrochemistry. *Science* **207,** 139–144 (1980).
2. Grätzel, M. Photoelectrochemical cells. *Nature* **414,** 338–344 (2001).
3. Walter, M. G. *et al.* Solar water splitting cells. *Chem. Rev.* **110,** 6446–6473 (2010).
4. Reece, S. Y. *et al.* Wireless solar water splitting using silicon-based semiconductors and earth-abundant catalysts. *Science* **334,** 645–648 (2011).
5. Wang, H. *et al.* Semiconductor heterojunction photocatalysts: design, construction, and photocatalytic performances. *Chem. Soc. Rev.* **43,** 5234–5244 (2014).
6. Hwang, Y. J., Boukai, A. & Yang, P. High density n-Si/n-TiO_2 core/shell nanowire arrays with enhanced photoactivity. *Nano Lett.* **9,** 410–415 (2009).
7. Hwang, Y. J., Wu, C. H., Hahn, C., Jeong, H. E. & Yang, P. Si/InGaN core/shell hierarchical nanowire arrays and their photoelectrochemical properties. *Nano Lett.* **12,** 1678–1682 (2012).
8. Liu, R. *et al.* Silicon nanowires as photoelectrodes for carbon dioxide fixation. *Angew. Chem. Int. Ed.* **51,** 6709–6712 (2012).
9. Mayer, M. T., Lin, Y., Yuan, G. & Wang, D. Forming heterojunctions at the nanoscale for improved photoelectrochemical water splitting by semiconductor materials: case studies on hematite. *Acc. Chem. Res.* **46,** 1558–1566 (2013).
10. Wu, Y., Yan, H. & Yang, P. Semiconductor nanowire array: potential substrates for photocatalysis and photovoltaics. *Top. Catal.* **19,** 197–202 (2002).
11. Liu, C., Dasgupta, N. P. & Yang, P. Semiconductor nanowires for artificial photosynthesis. *Chem. Mater.* **26,** 415–422 (2014).
12. Cui, Y., Wei, Q., Park, H. & Lieber, C. M. Nanowire nanosensors for highly sensitive and selective detection of biological and chemical species. *Science* **293,** 1289–1292 (2001).
13. Yan, R. *et al.* Nanowire-based single-cell endoscopy. *Nature Nanotech.* **7,** 191–196 (2012).
14. Tian, B., Kempa, T. J. & Lieber, C. M. Single nanowire photovoltaics. *Chem. Soc. Rev.* **38,** 16–24 (2009).
15. Tang, J., Huo, Z., Brittman, S., Gao, H. & Yang, P. Solution-processed core–shell nanowires for efficient photovoltaic cells. *Nature Nanotech.* **6,** 568–572 (2011).
16. Hochbaum, A. I. *et al.* Enhanced thermoelectric performance of rough silicon nanowires. *Nature* **451,** 163–167 (2008).
17. Cox, J. T. & Zhang, B. Nanoelectrodes: recent advances and new directions. *Annu. Rev. Anal. Chem.* **5,** 253–272 (2012).
18. Boettcher, S. W. *et al.* Photoelectrochemical hydrogen evolution using Si microwire arrays. *J. Am. Chem. Soc.* **133,** 1216–1219 (2011).
19. Hou, Y. *et al.* Bioinspired molecular co-catalysts bonded to a silicon photocathode for solar hydrogen evolution. *Nature Mater.* **10,** 434–438 (2011).
20. Esposito, D. V., Levin, I., Moffat, T. P. & Talin, A. A. H_2 evolution at Si-based metal–insulator–semiconductor photoelectrodes enhanced by inversion channel charge collection and H spillover. *Nature Mater.* **12,** 562–568 (2013).
21. Ji, L. *et al.* A silicon-based photocathode for water reduction with an epitaxial $SrTiO_3$ protection layer and a nanostructured catalyst. *Nature Nanotech.* **10,** 84–90 (2015).
22. Gorostiza, P., Allongue, P., Díaz, R., Morante, J. R. & Sanz, F. Electrochemical characterization of the open-circuit deposition of platinum on silicon from fluoride solutions. *J. Phys. Chem. B* **107,** 6454–6461 (2003).
23. Hochbaum, A. I., Fan, R., He, R. & Yang, P. Controlled growth of Si nanowire arrays for device integration. *Nano Lett.* **5,** 457–460 (2005).
24. Allen, J. E. *et al.* High-resolution detection of Au catalyst atoms in Si nanowires. *Nature Nanotech.* **3,** 168–173 (2008).
25. Koren, E. *et al.* Direct measurement of individual deep traps in single silicon nanowires. *Nano Lett.* **11,** 2499–2502 (2011).
26. Barton, E. E., Rampulla, D. M. & Bocarsly, A. B. Selective solar-driven reduction of CO_2 to methanol using a catalyzed p-GaP based photoelectrochemical cell. *J. Am. Chem. Soc.* **130,** 6342–6344 (2008).
27. Kumar, B., Smieja, J. M. & Kubiak, C. P. Photoreduction of CO_2 on p-type silicon using Re(bipy-But)$(CO)_3$Cl: photovoltages exceeding 600 mV for the selective reduction of CO_2 to CO. *J. Phys. Chem. C* **114,** 14220–14223 (2010).
28. Benson, E. E., Kubiak, C. P., Sathrum, A. J. & Smieja, J. M. Electrocatalytic and homogeneous approaches to conversion of CO_2 to liquid fuels. *Chem. Soc. Rev.* **38,** 89–99 (2009).
29. Appel, A. M. *et al.* Frontiers, opportunities, and challenges in biochemical and chemical catalysis of CO_2 fixation. *Chem. Rev.* **113,** 6621–6658 (2013).
30. Hori, Y. *et al.* Electrocatalytic process of CO selectivity in electrochemical reduction of CO_2 at metal electrodes in aqueous media. *Electrochim. Acta* **39,** 1833–1839 (1994).

Acknowledgements

This work was supported by the Director, Office of Science, Office of Basic Energy Sciences, Materials Sciences and Engineering Division, of the US Department of Energy (contract no. DE-AC02-05CH11231, Pchem). Y.S. is supported by graduate fellowship support from USTC-Suzhou Industrial Park. High-resolution transmission electron microscopy was performed at the National Center of Electron Microscopy (NCEM) in the Molecular Foundry at Lawrence Berkeley National Laboratory. The authors thank K. Sakimoto, J. Resasco, A. Wong, S. Eaton and J. Lim for discussions. The authors acknowledge the Marvell Nanofabrication Laboratory for use of their facilities.

Author contributions

Y.S., C.L. and P.Y. conceived and designed the experiments. Y.S., C.L., S.B. and J.T. fabricated the single-nanowire devices. Y.S. and C.L. performed the PEC measurements on single-nanowire devices. Y.S., C.L. and A.F. carried out the numerical calculation. Y.S. and Q.K. fabricated and characterized the nanowire array samples. N.K. carried out the high-resolution TEM imaging. Y.S., C.L. and P.Y. co-wrote the paper. All authors discussed the results and revised the manuscript.

Additional information

Supplementary information is available in the online version of the paper. Reprints and permissions information is available online at www.nature.com/reprints. Correspondence and requests for materials should be addressed to P.Y.

Competing financial interests

The authors declare no competing financial interests.

Methods

Growth of silicon nanowires. Heavily doped ($\rho = 0.01–0.05\ \Omega$ cm) p-type (boron) SOI wafers with the 3 μm device layer oriented ⟨111⟩ and 2 μm buried oxide layer were obtained from WRS Materials. The device layer was first thinned to 1.5 μm by thermal oxidation and subsequent etching in buffered hydrofluoric acid (BHF). The device layer was further doped with boron (Techneglas GS-139) at 1,050 °C for 10 h, followed by a second thermal oxidation and BHF etching. The resulting device layer was ~1 μm thick with a resistivity of <0.002 Ω cm. The Si electrodes were patterned by photolithography and anisotropic plasma etching (Surface Technology Systems) and then thermally oxidized to form a 300-nm-thick oxide. The bonding pads were defined by photolithography and anisotropic plasma etching of the oxide (Plasma-Therm PK-12 RIE). The catalysts for VLS growth were defined by photolithography, anisotropic plasma etching of the oxide and subsequent electron-beam evaporation of gold (150 nm). The isolated silicon nanowires were grown at 875 °C for 10–15 min with $SiCl_4$ as the precursor and 10% hydrogen in argon as the reducing agent.

Device fabrication after growth. The as-grown isolated silicon nanowires were etched in BHF for 30 s and subsequently soaked in gold etchant (Transene) for 30 min. The nanowires were then thermally oxidized at 1,000 °C for 1 h, followed by etching in BHF. The boron doping process was split into two parts. First, boron was predeposited at the nanowire surface at 750 °C for 1 h, with 1% BCl_3 in argon as the precursor and 10% hydrogen in argon as the reducing agent. Second, the boron atoms at the nanowire surface were driven into the nanowire at 1,000 °C for 5 h in vacuum. The resulting boron doping level of the single nanowires was estimated to be $\sim 2 \times 10^{17}$ cm^{-3}. This estimation is based on the resistivity of the SOI control chip, which was approximated by four-probe measurements. The key steps used in the n^+ layer fabrication are as follows (see Supplementary Section 'Fabrication of the n^+p-Si single-nanowire device' for details). The p-Si nanowires were first thermally oxidized at 1,000 °C for 1 h, then coated with ~1 μm of I-line photoresist at the base of the nanowires. Second, BHF was used to etch the oxide on the nanowire upper exposed part, followed by I-line removal in acetone. Third, a Si handle wafer was spin-coated with arsenic-containing spin-on dopant (SOD) (Filmtronics) and baked at 150 °C for 30 min. The device chip was then placed on the SOD-coated silicon wafer, and annealed at 900 °C for 4 min in an N_2 atmosphere to form an n^+ layer at the surface of the nanowire. Fourth, SU-8 dissolved in ethyl acetate was dropcast onto the device chip, resulting in an ~3-μm-thick SU-8 layer at the base of the device chip. With the SU-8 at the bonding pad scratched to expose the electrode's surface, the chip was baked to harden the SU-8. Finally, after a quick etching in BHF, the device chip was soaked in a solution containing 0.1 M HF and 0.2 mM K_2PtCl_6 for 3 min to deposit platinum on the nanowire surface[22].

PEC measurement. A 150 W xenon arc lamp (Newport Corporation) with an AM1.5G filter was used to characterize the PEC response of the single-nanowire devices. As a top-illumination measurement, the angle between the incident light and the axis of the single nanowire was smaller than 3°. The light intensity was calibrated using a silicon photodiode referenced to a NREL calibrated silicon photodiode. All PEC measurements were carried out in a two-electrode configuration. A platinum wire operated as the counterelectrode, and its electrochemical potential was immediately calibrated with Ag/AgCl (0.1 M KCl) after the PEC measurement (Supplementary Fig. 4). A PDMS chamber was used to define the reactor space, where the nanowire device was immersed in 0.1 M aq. K_2SO_4 adjusted to pH ~2 using H_2SO_4. *I–V* characterization was performed with a Keithley 2636 source-measure unit (SMU) and the typical potential sweep rate was 10 mV s^{-1}. The open-circuit instrumental noise current level was less than 0.5 pA.